Nano Research 2015, 8(1): 281–287
DOI 10.1007/s12274-014-0673-y
Research Article
ISSN 1998-0124
CN 11-5974/O4

MoS_2-wrapped silicon nanowires for photoelectrochemical water reduction

Liming Zhang[1,†,§], Chong Liu[1,§], Andrew Barnabas Wong[1,4], Joaquin Resasco[2], and Peidong Yang[1,3,4] (✉)

[1] *Department of Chemistry, University of California, Berkeley, CA 94720, USA*
[2] *Department of Chemical Engineering, University of California, Berkeley, CA 94720, USA*
[3] *Department of Materials Science and Engineering, University of California, Berkeley, CA 94720, USA*
[4] *Materials Sciences Division, Lawrence Berkeley National Laboratory, Berkeley, CA 94720, USA*
[†] *Present address: Department of Materials Science and Engineering, Stanford University, Stanford, CA 94305, USA*
[§] *These authors contributed equally to this work.*

Received: 3 November 2014
Revised: 26 November 2014
Accepted: 30 November 2014

KEYWORDS
MoS_2,
Si nanowire array,
coaxial heterostructure,
photoelectrochemistry,
hydrogen evolution reaction (HER)

ABSTRACT

Integration of molybdenum disulfide (MoS_2) onto high surface area photocathodes is highly desired to minimize the overpotential for the solar-powered hydrogen evolution reaction (HER). Semiconductor nanowires (NWs) are beneficial for use in photoelectrochemistry because of their large electrochemically available surface area and inherent ability to decouple light absorption and the transport of minority carriers. Here, silicon (Si) NW arrays were employed as a model photocathode system for MoS_2 wrapping, and their solar-driven HER activity was evaluated. The photocathode is made up of a well-defined $MoS_2/TiO_2/Si$ coaxial NW heterostructure, which yielded photocurrent density up to 15 mA/cm^2 (at 0 V vs. the reversible hydrogen electrode (RHE)) with good stability under the operating conditions employed. This work reveals that earth-abundant electrocatalysts coupled with high surface area NW electrodes can provide performance comparable to noble metal catalysts for photocathodic hydrogen evolution.

1 Introduction

The vision of utilization of hydrogen as a future energy source requires a sustainable, highly efficient, and cost-effective production method [1]. To use renewable energy to produce hydrogen fuel, solar-driven water splitting is one of the most promising approaches [2, 3]. Effective photelectrochemical (PEC) water splitting devices must be able to absorb a large fraction of incident sunlight, generate high photocurrent with sufficient photovoltage, and exhibit long-term stability. One challenge in designing such a device is to reduce the reaction overpotential, by increasing the reaction kinetics on the surface. While existing noble metal catalysts, such as Pt, are highly active at catalyzing the hydrogen evolution reaction (HER) [4, 5], the high cost

Address correspondence to p_yang@berkeley.edu

of these materials limits the economic viability of their use for hydrogen production. The intensive search for earth-abundant, inexpensive, and nontoxic catalysts with comparable performance for the HER has led to significant progress in the development of new catalysts, including metal alloys [6, 7], nitrides [8], borides [9], carbides [9, 10], chalcogenides [11–16], and phosphides [17]. In particular, metal chalcogenides, such as molybdenum sulfide (MoS_x), are an exciting group of HER catalysts that exhibit promising activity in both crystalline and amorphous forms, as well as in the form of grafted molecular clusters [11, 12, 18–20]. Despite the considerable efforts dedicated to investigating and optimizing the catalytic activity of various MoS_x materials, the effective integration of MoS_x onto photocathodes is still a challenge. To achieve high geometric area-normalized HER activity, it is necessary to carefully engineer MoS_x functional nanostructures to maximize the density of active sites, which have been identified both theoretically [21, 22] and experimentally [11, 12, 23, 24] to be the uncoordinated sulfur edge sites.

High surface area photoelectrodes, such as semiconductor nanowire (NW) arrays, are attractive because of their large semiconductor/electrolyte interfacial area, enhanced light scattering effect, and efficient transport of charge carriers [25–27]. Silicon (Si), with bandgap of 1.12 eV, is a promising candidate as a light-absorber due to its relatively low cost, excellent carrier transport properties, and suitable band edge with respect to HER potential [27]. As atomically thin MoS_2 has limited light absorption, the successful integration of MoS_2 with semiconductor NWs constitutes an ideal system for PEC hydrogen production.

In this work, using a p-Si NW array as scaffold, a well-defined MoS_2/TiO_2/Si NW integrated coaxial heterostructure was constructed as a model photocathode system for PEC hydrogen generation. Multilayer MoS_2 with a small domain size of ~10 nm was uniformly wrapped on the surface of the NWs, exposing a high density of active uncoordinated edge sites. An onset of photocurrent at ~0.30 V vs. the reversible hydrogen electrode (RHE), together with a short-circuit current density of 15 mA/cm^2 under simulated 1 sun illumination was achieved. Additionally, this functional device exhibits good stability under the operating conditions employed. This system demonstrates the principle that earth-abundant electrocatalysts coupled with high surface area NW electrodes can provide performance comparable to noble metal catalysts for photocathodic hydrogen evolution. This principle could serve as a guide for future studies in the field of solar-powered chemical fuel production, by offering an additional dimension for device engineering through the benefits of the NW morphology.

2 Results and discussion

Since metal oxide overlayers can assist in preserving the photoresponse of Si [28], in our study Si/TiO_2 core–shell structures were prepared via atomic layer deposition (ALD) of 30 nm of crystalline TiO_2 on the NW surface at 573 K. The MoS_2 layer was synthesized by thermolysis of ammonium tetrathiomolybdate ($(NH_4)_2MoS_4$) at low temperature [29, 30]. $(NH_4)_2MoS_4$ was dissolved in an organic solvent and drop-casted onto the NW surface (additional details are provided in the Electronic Supplementary Material (ESM)). After drop-casting, the coated NWs were annealed at 573–673 K in a N_2/H_2 (80/20 sccm) atmosphere at ambient pressure to form MoS_2.

A single TiO_2/Si NW wrapped with MoS_2 was characterized by high-angle annular dark field (HAADF) imaging (Fig. 1(a)). The MoS_2 and TiO_2 shells appear brighter, as Ti and Mo atoms located in the shell have a higher atomic number than the Si atoms in the core. High-resolution transmission electron microscopy (HRTEM) revealed multiple layers of MoS_2 on the NW surface, as evidenced by the lattice fringes with a spacing of 0.62 nm, in agreement with the expected MoS_2 interlayer distance of 0.614 nm (Fig. 1(b)) [31, 32]. The crystallinity of MoS_2 depends strongly on the annealing temperature, with increasing temperature resulting in higher crystallinity (Fig. S1 in the ESM). Although the surface is mostly covered with MoS_2 basal planes, the domain size is smaller than 10 nm and abundant crystal edges of MoS_2 are evident (indicated by the red arrows in Fig. 1(b)). Relative to MoS_2 coated on planar electrode surfaces [18, 33], this core–shell structure exposes more MoS_2 edges because of the large surface area afforded by the NW morphology. Further analysis of the elemental

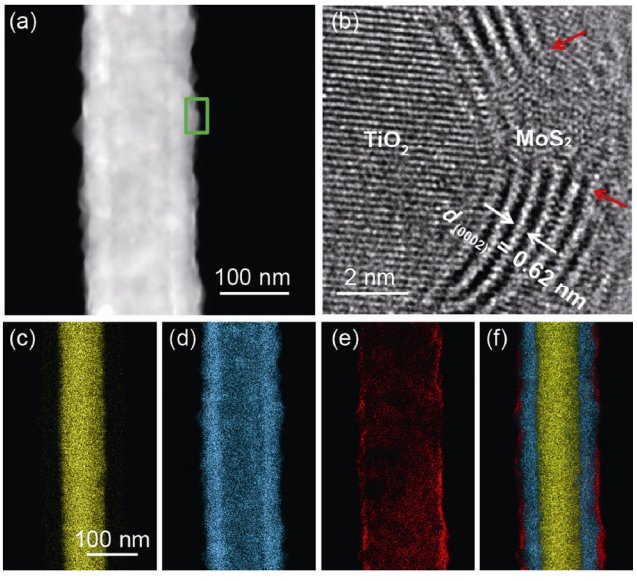

Figure 1 (a) HAADF image of the $MoS_2/TiO_2/Si$ coaxial structure on a single NW. (b) HRTEM image taken at the MoS_2/TiO_2 interface as shown in the green box of (a). The lattice fringes show a spacing of 0.62 nm between adjacent layers, which is in agreement with the expected MoS_2 interlayer distance. The red arrows indicate the edge of a MoS_2 cluster where HER-active MoS_2 edge sites are likely exposed on the NW surface. (c)–(f) EDS elemental mapping along a single NW, which shows the elemental distribution of (c) Si, (d) Ti, (e) Mo, and the combined signal of (f) Mo/Ti/Si, demonstrating the well-defined integrated coaxial heterostructure of $MoS_2/TiO_2/Si$ NW.

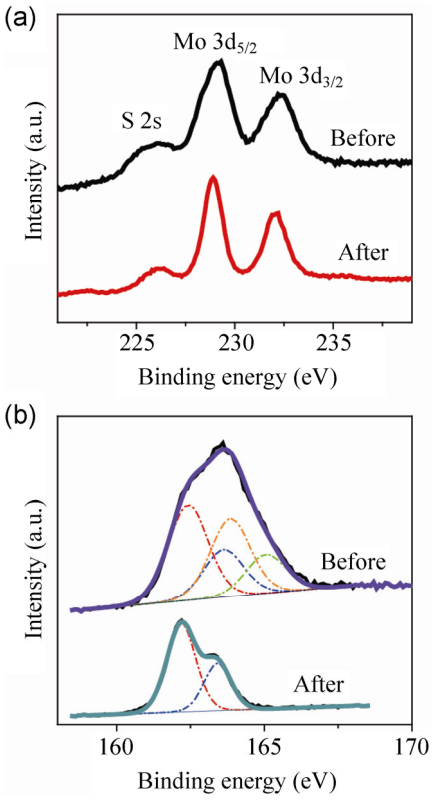

Figure 2 XPS characterization of (a) Mo and (b) S signals in the MoS_x cocatalyst before and after annealing. The Mo 3d region shows the Mo oxidation state is 4+ before and after annealing while the S 2p region shows a transition from MoS_3 to MoS_2.

distribution was obtained from energy dispersive X-ray spectroscopy (EDS) mapping. The elemental map shows a homogenous distribution of Si in the core (Fig. 1(c)), Ti in the inner shell (Fig. 1(d)), and a thin layer of Mo in the outer shell (Fig. 1(e)). The combined elemental mapping in Fig. 1(f) demonstrates a well-defined coaxial heterostructure of $MoS_2/TiO_2/Si$ along a single NW. The uniform coating of MoS_2 distributes the solar-generated electron flux evenly along the semiconductor light-absorber. The effective utilization of the high surface area of the NW decreases the surface flux of electrons, leading to a reduced HER kinetic overpotential.

Additional characterization was performed to understand the nature of the synthesized MoS_2, from which deeper insight into the performance may be gained. Thermolysis of $(NH_4)_2MoS_4$ at low temperature in the presence of H_2 will result in the conversion initially to MoS_3 and finally to MoS_2 [29]. X-ray photoelectron spectroscopy (XPS) (Fig. 2) and Raman spectroscopy (Fig. S2 in the ESM) were used to investigate the chemical states of Mo and S before and after annealing. The binding energy of the Mo $3d_{5/2}$ photoelectron peak remained constant (229.2 eV) before and after annealing, indicating a 4+ oxidation state for Mo [13]. The S 2p region of MoS_x before annealing shows two doublets, consistent with that seen for MoS_3 amorphous catalysts [13]. The doublet at lower binding energy (162.2 and 163.4 eV) is attributed to S^{2-} at the basal plane, characteristic of MoS_2. The doublet at higher binding energy (163.8 and 165.0 eV) is attributed to S_2^{2-} at the bridge sites. After annealing, only the doublet at lower binding energy corresponding to MoS_2 is observed. These results demonstrate that this low temperature annealing process is a simple method for the synthesis of stoichiometric MoS_2 catalysts with small domain sizes and uniform coverage, even on highly corrugated surfaces.

The electrocatalytic performance of MoS_2 layers

was first evaluated using planar p^+-Si substrate as an electrode. Different volumes of precursor solution, corresponding to different loadings of the MoS_2 cocatalyst, were drop-casted onto the electrode surface, followed by annealing at 673 K in a N_2/H_2 atmosphere at ambient pressure. The TiO_2 interlayer was required to achieve stable current; otherwise, the underlying Si will be gradually oxidized, leading to a decrease in activity (Fig. S3 in the ESM). The catalytic performance was measured using iR-compensated linear scan voltammetry in 0.5 M H_2SO_4 electrolyte in a three-electrode configuration. Onset of cathodic current was observed at approximately –0.20 V vs. the reversible hydrogen electrode (RHE) (Fig. 3(a)). The cathodic current increased with increasing loading of MoS_2 and exhibited a Tafel slope of 75–84 mV per decade (Fig. 3(b)). The apparent exchange current densities j_0 were obtained from the Tafel plots and are summarized in Table S1 (in the ESM). The Tafel slope observed here compares favorably with MoS_2 synthesized by chemical vapor deposition (CVD) on glassy carbon electrodes [18, 34]. After evaluating the dependence of HER activity on the MoS_2 loading density, the optimal condition was applied to the NW

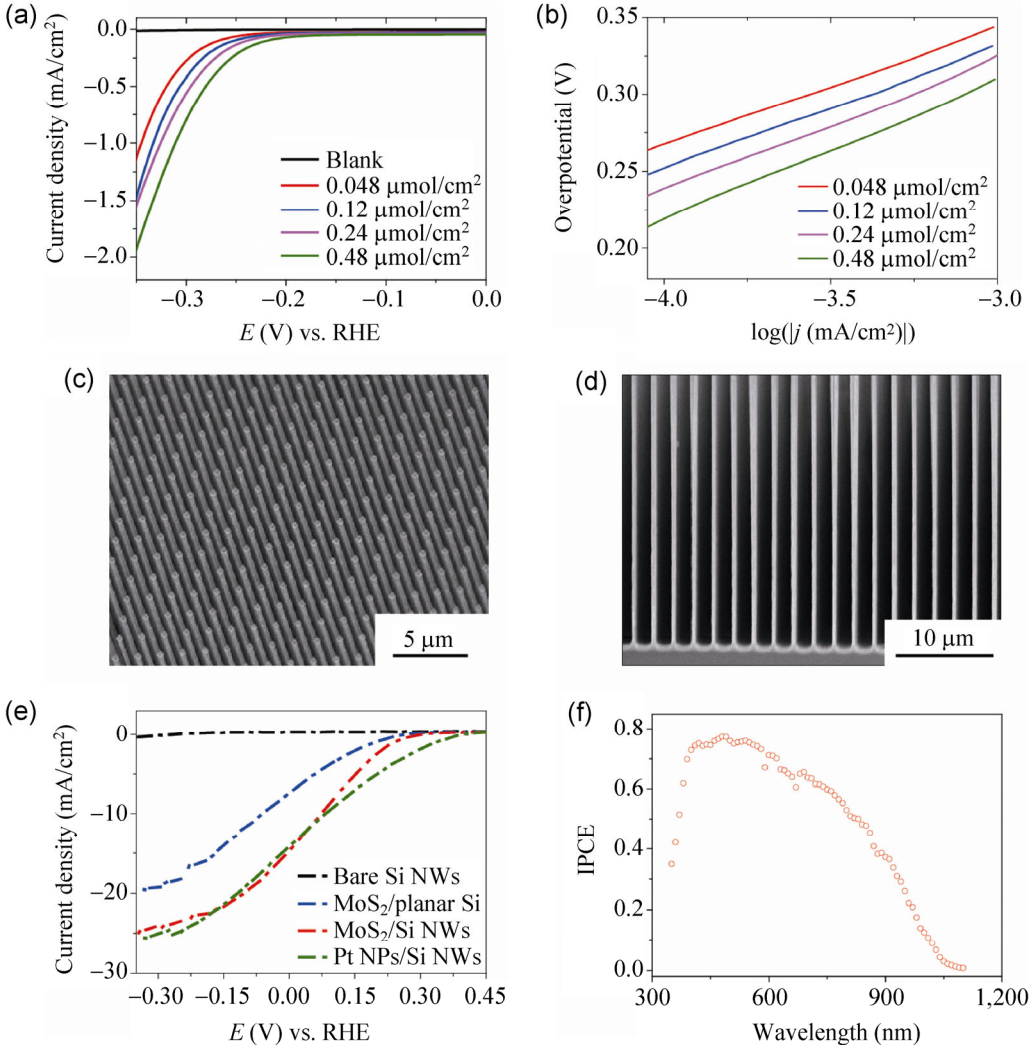

Figure 3 (a) and (b) Electrochemical performance of MoS_2 catalysts in 0.5 M H_2SO_4: (a) Linear sweep voltammograms and (b) Tafel plots for TiO_2-coated p^+-Si planar surface with different MoS_2 loadings. (c) 45° tilt and (d) cross-sectional SEM images of as-grown Si NW arrays. (e) Comparison of HER performance (under 100 mW/cm^2 simulated AM 1.5 G irradiation) of Si NW array photocathodes coated with MoS_2 to an MoS_2 coated planar Si substrate, and a Si NW array loaded with Pt nanoparticles. (f) Spectral response (incident photon to current conversion efficiency (IPCE)) of Si NW arrays after coating with MoS_2 layers.

photoelectrodes for subsequent PEC investigation.

To evaluate the impact of MoS_2 cocatalyst deposition on the solar-to-hydrogen activity of the Si NW photocathodes, PEC measurements were performed under the same conditions as the electrochemical measurements described above. A well-defined high surface area Si NW array electrode was fabricated via deep reactive ion etching (DRIE) (experimental details are provided in the ESM). The scanning electron micrographs are shown in Fig. 3(c) and 3(d). The etched NW arrays are approximately 30 μm in length and 800 nm in diameter, and are arranged on a square lattice with periodicity of 2 μm. In order to achieve a positive photovoltage, a heavily doped n^+ emitter layer was diffused into the surface region of Si NWs via rapid temperature annealing at 1173 K for 3 min, using arsenic (As) as an n-type dopant. Following the procedure outlined above, a $MoS_2/TiO_2/n^+p$-Si NW coaxial heterostructure was created from the Si NW array. For comparison, $Pt/TiO_2/n^+p$-Si NW was also fabricated by sputtering Pt nanoparticles onto the NW surface (Fig. S4 in the ESM). The PEC performance of these photoelectrodes was tested under identical conditions, using 100 mW/cm^2 simulated AM 1.5 G irradiation. Figure 3(e) shows the activity comparison of Si photocathodes before and after deposition of MoS_2. Si NW arrays exhibit nearly no photo-activity in the absence of a cocatalyst. When MoS_2 was deposited onto the NW surface, the onset of photocurrent shifted substantially to a more positive potential (~0.30 V vs. RHE), only 100 mV cathodic of the Pt nanoparticle decorated electrode. For the affordable application of overall water splitting by coupling of dual light absorbers, a current density on the order of 10 mA/cm^2 is necessary [20]. The MoS_2 layers wrapped Si NW array photocathode provides a current density of ~15 mA/cm^2 at 0 V vs. RHE, indicating that this photocathode can be an affordable integrated water-splitting system.

To study the impact of NW surface area on the required catalytic activity, an equal loading of MoS_2 was deposited on the surface of a planar TiO_2/n^+p-Si electrode. As shown in Fig. 3(e), the photo-activity was substantially improved in the Si NW array, indicating that increasing the surface area will decrease the surface flux of electrons, leading to a lower requirement for the catalytic activity on the surface. Figure 3(f) shows the typical spectral response for $MoS_2/TiO_2/n^+p$-Si NWs (experimental details are provided in the ESM). The external quantum efficiency reaches a maximum at 500 nm, consistent with the external quantum efficiency observed for Si wires coated with a thin layer of Pt nanoparticles [4]. The maximum external quantum efficiency is larger than 0.75, ~25% higher than previously reported for Ni–Mo coated Si wire arrays [7].

Another important criterion for PEC energy conversion is the long-term stability of the photoelectrode under actual operating conditions. The short-term stability of the coaxial MoS_2/TiO_2/Si NW structure and its faradaic efficiency for hydrogen reduction were evaluated by chronoamperometry. The potential of the photocathode was held at –0.33 V vs. RHE under 100 mW/cm^2 simulated AM 1.5 G irradiation, and both the photocurrent and hydrogen gas concentration in the Ar carrier gas were monitored. Bubbles were continuously evolved from photocathode, and the accumulation and release of these bubbles led to the observed variations in photocurrent over the duration of the measurement. The photocurrent of the coaxial MoS_2/TiO_2/Si NW structure remained at approximately 21 mA/cm^2 for 75 min without degradation (Fig. 4), and the faradaic efficiency for hydrogen evolution to H_2 was found to be ~100% (more details are provided in the ESM and Fig. S5). This result shows that the coaxial MoS_2/TiO_2/Si NWs are stable and are indeed reducing water into H_2.

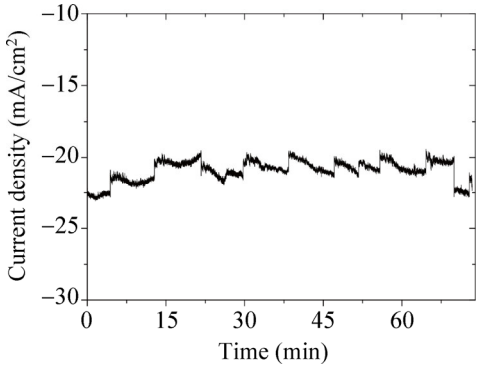

Figure 4 Stability test of MoS_2 wrapped Si NW array. Current vs. time during the controlled potential photoelectrolysis under 100 mW/cm^2 simulated AM 1.5 G irradiation at –0.33 V vs. RHE.

3 Conclusions

This work shows the feasibility of functionalizing a Si NW array photocathode with a MoS_2 cocatalyst to drive solar hydrogen production. The exploration of the earth-abundant catalyst MoS_2 and its application in high surface area Si NW array electrodes establishes a general strategy to replace precious metal cocatalysts for efficient and affordable solar-to-fuel application at a large scale.

Acknowledgements

This work was supported by the Director, Office of Science, Office of Basic Energy Sciences, Materials Science and Engineering Division, U.S. Department of Energy under Contract No. DE-AC02-05CH11231 (P-Chem). J.R. gratefully acknowledges the support of the National Science Foundation Graduate Research Fellowship Program (NSF GRFP) under Grant No. DGE-0802270.

Electronic Supplementary Material: Supplementary material (experimental details, additional TEM, Raman data, stability measurement, and calculations of electrochemical performance) is available in the online version of this article at http://dx.doi.org/10.1007/s12274-014-0673-y.

References

[1] Turner, J. A. Sustainable hydrogen production. *Science* **2004**, *305*, 972–974.

[2] Walter, M. G.; Warren, E. L.; McKone, J. R.; Boettcher, S. W.; Mi, Q.; Santori, E. A.; Lewis, N. S. Solar water splitting cells. *Chem. Rev.* **2010**, *110*, 6446–6473.

[3] Lewis, N. S.; Nocera, D. G. Powering the planet: Chemical challenges in solar energy utilization. *Proc. Natl. Acad. Sci. U.S.A.* **2006**, *103*, 15729–15735.

[4] Boettcher, S. W.; Warren, E. L.; Putnam, M. C.; Santori, E. A.; Turner-Evans, D.; Kelzenberg, M. D.; Walter, M. G.; McKone, J. R.; Brunschwig, B. S.; Atwater, H. A.; et al. Photoelectrochemical hydrogen evolution using Si microwire arrays. *J. Am. Chem. Soc.* **2011**, *133*, 1216–1219.

[5] Dasgupta, N. P.; Liu, C.; Andrews, S.; Prinz, F. B.; Yang, P. Atomic layer deposition of platinum catalysts on nanowire surfaces for photoelectrochemical water reduction. *J. Am. Chem. Soc.* **2013**, *135*, 12932–12935.

[6] Reece, S. Y.; Hamel, J. A.; Sung, K.; Jarvi, T. D.; Esswein, A. J.; Pijpers, J. J. H.; Nocera, D. G. Wireless solar water splitting using silicon-based semiconductors and earth-abundant catalysts. *Science* **2011**, *334*, 645–648.

[7] McKone, J. R.; Warren, E. L.; Bierman, M. J.; Boettcher, S. W.; Brunschwig, B. S.; Lewis, N. S.; Gray, H. B. Evaluation of Pt, Ni, and Ni–Mo electrocatalysts for hydrogen evolution on crystalline Si electrodes. *Energy Environ. Sci.* **2011**, *4*, 3573–3583.

[8] Chen, W. F.; Sasaki, K.; Ma, C.; Frenkel, A. I.; Marinkovic, N.; Muckerman, J. T.; Zhu, Y. M.; Adzic, R. R. Hydrogen-evolution catalysts based on non-noble metal nickel–molybdenum nitride nanosheets. *Angew. Chem. Inter. Ed.* **2012**, *51*, 6131–6135.

[9] Vrubel, H.; Hu, X. Molybdenum boride and carbide catalyze hydrogen evolution in both acidic and basic solutions. *Angew. Chem. Inter. Ed.* **2012**, *124*, 12875–12878.

[10] Chen, W. F.; Wang, C.-H.; Sasaki, K.; Marinkovic, N.; Xu, W.; Muckerman, J. T.; Zhu, Y.; Adzic, R. R. Highly active and durable nanostructured molybdenum carbide electrocatalysts for hydrogen production. *Energy Environ. Sci.* **2013**, *6*, 943–951.

[11] Jaramillo, T. F.; Jorgensen, K. P.; Bonde, J.; Nielsen, J. H.; Horch, S.; Chorkendorff, I. Identification of active edge sites for electrochemical H_2 evolution from MoS_2 nanocatalysts. *Science* **2007**, *317*, 100–102.

[12] Kibsgaard, J.; Chen, Z. B.; Reinecke, B. N.; Jaramillo, T. F. Engineering the surface structure of MoS_2 to preferentially expose active edge sites for electrocatalysis. *Nat. Mater.* **2012**, *11*, 963–969.

[13] Merki, D.; Hu, X. L. Recent developments of molybdenum and tungsten sulfides as hydrogen evolution catalysts. *Energy Environ. Sci.* **2011**, *4*, 3878–3888.

[14] Voiry, D.; Yamaguchi, H.; Li, J. W.; Silva, R.; Alves, D. C. B.; Fujita, T.; Chen, M. W.; Asefa, T.; Shenoy, V. B.; Eda, G.; et al. Enhanced catalytic activity in strained chemically exfoliated WS_2 nanosheets for hydrogen evolution. *Nat. Mater.* **2013**, *12*, 850–855.

[15] Sun, Y. J.; Liu, C.; Grauer, D. C.; Yano, J. K.; Long, J. R.; Yang, P. D.; Chang, C. J. Electrodeposited cobalt–sulfide catalyst for electrochemical and photoelectrochemical hydrogen generation from water. *J. Am. Chem. Soc.* **2013**, *135*, 17699–17702.

[16] Kong, D. S.; Cha, J. J.; Wang, H. T.; Lee, H. R.; Cui, Y. First-row transition metal dichalcogenide catalysts for hydrogen evolution reaction. *Energy Environ. Sci.* **2013**, *6*, 3553–3558.

[17] Popczun, E. J.; McKone, J. R.; Read, C. G.; Biacchi, A. J.; Wiltrout, A. M.; Lewis, N. S.; Schaak, R. E. Nanostructured nickel phosphide as an electrocatalyst for the hydrogen evolution reaction. *J. Am. Chem. Soc.* **2013**, *135*, 9267–9270.

[18] Yu, Y. F.; Huang, S. Y.; Li, Y. P.; Steinmann, S. N.; Yang, W. T.; Cao, L. Y. Layer-dependent electrocatalysis of MoS_2 for hydrogen evolution. *Nano Lett.* **2014**, *14*, 553–558.

[19] Karunadasa, H. I.; Montalvo, E.; Sun, Y. J.; Majda, M.; Long, J. R.; Chang, C. J. A molecular MoS_2 edge site mimic for catalytic hydrogen generation. *Science* **2012**, *335*, 698–702.

[20] Hou, Y. D.; Abrams, B. L.; Vesborg, P. C. K.; Bjorketun, M. E.; Herbst, K.; Bech, L.; Setti, A. M.; Damsgaard, C. D.; Pedersen, T.; Hansen, O.; et al. Bioinspired molecular co-catalysts bonded to a silicon photocathode for solar hydrogen evolution. *Nat. Mater.* **2011**, *10*, 434–438.

[21] Hinnemann, B.; Moses, P. G.; Bonde, J.; Jorgensen, K. P.; Nielsen, J. H.; Horch, S.; Chorkendorff, I.; Norskov, J. K. Biornimetic hydrogen evolution: MoS_2 nanoparticles as catalyst for hydrogen evolution. *J. Am. Chem. Soc.* **2005**, *127*, 5308–5309.

[22] Norskov, J. K.; Bligaard, T.; Rossmeisl, J.; Christensen, C. H. Towards the computational design of solid catalysts. *Nat. Chem.* **2009**, *1*, 37–46.

[23] Zhou, H.; Yu, F.; Liu, Y.; Zou, X.; Cong, C.; Qiu, C.; Yu, T.; Yan, Z.; Shen, X.; Sun, L. Thickness-dependent patterning of MoS_2 sheets with well-oriented triangular pits by heating in air. *Nano Res.* **2013**, *6*, 703–711.

[24] Huang, Y.; Wu, J.; Xu, X.; Ho, Y.; Ni, G.; Zou, Q.; Koon, G.; Zhao, W.; Neto, A.; Eda, G. An innovative way of etching MoS_2: Characterization and mechanistic investigation. *Nano Res.* **2013**, *6*, 200–207.

[25] Liu, C.; Dasgupta, N. P.; Yang, P. D. Semiconductor nanowires for artificial photosynthesis. *Chem. Mater.* **2014**, *26*, 415–422.

[26] Yang, P. D.; Yan, R. X.; Fardy, M. Semiconductor nanowire: What's next? *Nano Lett.* **2010**, *10*, 1529–1536.

[27] Boettcher, S. W.; Spurgeon, J. M.; Putnam, M. C.; Warren, E. L.; Turner-Evans, D. B.; Kelzenberg, M. D.; Maiolo, J. R.; Atwater, H. A.; Lewis, N. S. Energy-conversion properties of vapor–liquid–solid-grown silicon wire-array photocathodes. *Science* **2010**, *327*, 185–187.

[28] Seger, B.; Pedersen, T.; Laursen, A. B.; Vesborg, P. C.; Hansen, O.; Chorkendorff, I. Using TiO_2 as a conductive protective layer for photocathodic H_2 evolution. *J. Am. Chem. Soc.* **2013**, *135*, 1057–1064.

[29] Brito, J. L.; Ilija, M.; Hernández, P. Thermal and reductive decomposition of ammonium thiomolybdates. *Thermochim. Acta* **1995**, *256*, 325–338.

[30] Liu, K. K.; Zhang, W. J; Lee, Y. H.; Lin, Y. C.; Chang, M. T.; Su, C. Y.; Chang, C. S.; Li, H.; Shi, Y. M.; Zhang, H.; et al. Growth of large-area and highly crystalline MoS_2 thin layers on insulating substrates. *Nano Lett.* **2012**, *12*, 1538–1544.

[31] Tributsch, H.; Bennett, J. C. Electrochemistry and photochemistry of MoS_2 layer crystals. *J. Electroanal. Chem.* **1977**, *81*, 97–111.

[32] Gomez, A.; van der Zant, H.; Steele, G. Folded MoS_2 layers with reduced interlayer coupling. *Nano Res.* **2014**, *7*, 1–7.

[33] Seger, B.; Laursen, A. B.; Vesborg, P. C. K.; Pedersen, T.; Hansen, O.; Dahl, S.; Chorkendorff, I. Hydrogen production using a molybdenum sulfide catalyst on a titanium-protected n^+p-silicon photocathode. *Angew Chem. Int. Ed.* **2012**, *5*, 9128–9131.

[34] Kong, D. S.; Wang, H. T.; Cha, J. J.; Pasta, M.; Koski, K. J.; Yao, J.; Cui, Y. Synthesis of MoS_2 and $MoSe_2$ films with vertically aligned layers. *Nano Lett.* **2013**, *13*, 1341–1347.